Master's thesis

NTNU
Norwegian University of Science and Technology
Faculty of Information Technology and Electrical Engineering
Department of Electronic Systems

Ådne Gimse Estenstad

Imaging of Subsurface Injectite Structures

Master's thesis in Electronics Systems Design and Innovation
Supervisor: Espen Birger Raknes
July 2019

NTNU
Norwegian University of
Science and Technology

Abstract

The work in this thesis has focused on seismic imaging of subsurface injectite structures. These structures have a non-uniform geometry that can make imaging difficult. Areas of interest for this thesis involves; importance of model detail in the migration, acquisition geometry and type of migration (elastic versus acoustic). The thesis aimed at imaging these structures with three different acquisition geometries; the conventional streamer, the SOR (source over receiver) and the OBS (ocean bottom survey). Synthetic data was generated through an elastic finite difference process, granting a number of shot gathers for each acquisition geometry. The shot gathers were FK-filtered before being migrated by an RTM (reverse time migration). Both an acoustic and an elastic RTM were analyzed. This process granted a subsurface image. A k-space filter was also applied.

The elastic migration granted satisfactory results for all acquisition geometries. However, in the case of the conventional streamer geometry and the SOR geometry, the acoustic migration struggled to return the reflections to their true subsurface position. This points to an importance of elastic information when it comes to the imaging of subsurface injectite structures.

The detail of the model used in the migration was also analyzed. Four different models were considered; a uniform model, a gradient model, a layered model, and the true subsurface model used in the finite difference method. The results indicate that model detail is of great importance when injectite structures are to be imaged. An increased model detail significantly increased the detail of the subsurface image depicting the injectite structures.

The SOR geometry was of special interest in this thesis. There has been speculation that the increase in near offset information in comparison to the conventional streamer might contribute to a better subsurface image of the injectite structures. In this thesis, when an elastic migration was applied, the SOR geometry outperformed the conventional streamer geometry. The results indicate that there might be advantages to using the SOR geometry in place of the conventional streamer geometry when imaging subsurface injectite structures.

Sammendrag

Arbeidet i denne masteroppgaven har fokusert på seismisk avbildning av injektittstrukturer. Disse strukturene har en ikke-uniform geometri som kan gjøre avbildning utfordrende. Interesseområder for denne masteroppgaven inkluderer; viktighet av nøyaktighet i migrasjonsmodellen, innsamlingsgeometri og type migrasjon (elastisk mot akustisk). Masteroppgaven var siktet på avbildning av injektittstrukturene ved bruk av tre forskjellige innsamlingsgeometrier; en konvensjonell streamer geometri, en kilde over mottager streamer geometri (SOR) og en havbunnskabel geometri (OBS). Syntetisk data ble generert gjennom en finite difference prosess. Dette ga et nummer av skuddsamlinger for hver innsamlingsgeometri. Skuddsamlingene ble FK-filtrert og deretter ble skuddsamlingene migrert med en RTM. Både en akustisk og en elastisk RTM ble tatt i bruk. Denne prosessen ga et bilde av undergrunnen. En todimensjonal k-rom filtrering ble deretter anvendt for å fremheve injektittstrukturene.

Bruk av den elastiske migrasjonen ga tilfredsstillende resultater for samtlige innsamlingsgeometrier. I tilfellet av en konvensjonell streamer geometri og en SOR geometri, så man at en akustisk migrasjon slet med å returnere refleksjonene til deres faktiske undergrunnsposisjon. Disse resultatene antyder at elastisk informasjon spiller en viktig rolle når det kommer til avbildning av injektittstrukturer.

Grad av detalj brukt i migrasjonsmodellen ble også undersøkt i denne masteroppgaven. Fire forskjellige migrasjonsmodeller ble undersøkt; en uniform modell, en gradientmodell, en lagdelt modell og den virkelige modellen brukt i den syntetiske datagenerasjonen. Resultatene indikerer at modelldetalj er viktig når det kommer til avbildning av injektittstrukturer. En økt modelldetalj ga en betydelig økt detalj i avbildningen av injektittstrukturene.

SOR geometrien var av spesiell interesse i denne masteroppgaven. Det har blitt spekulert at geometriens økte mengde nær-offset data kan bære fordeler over en konvensjonell streamer geometri når det kommer til avbildning av injektittstrukturer. I denne analysen, når en elastisk migrasjon ble benyttet, så vi at SOR geometrien ga bedre bilder av injektittstrukturene enn det den konvensjonelle streamer geometrien gjorde. Resultatene indikerer at det kan være visse fordeler ved å bruke en SOR geometri over en konvensjonell streamer geometri når det kommer til avbildning av injektittstrukturer i undergrunnen.

Acknowledgment

Firstly, I would like to thank my thesis supervisor Espen Raknes, from the Norwegian University of Science and Technology (NTNU), for assistance and inspiration. I also would like to thank Antonio Grippa for providing the geological model used in this analysis.

Contents

1 Introduction

Seismic imaging has for a long time played an important role in the uncovering of subsurface hydrocarbon resources. Due to the expensive nature of offshore exploration, subsurface imaging has become a crucial tool in the search of new hydrocarbon rich areas.

Through many years of seismic imaging, many new methods emerged with their own advantages and drawbacks. The conventional streamer, the ocean bottom survey (OBS) and more recently the source over receiver (SOR) method have all been used in the pursuit of hydrocarbon deposits.

Recently, high contrast injectite anomalies have been targeted in seismic exploration. These structures have previously been overlooked in the pursuit of conventional hydrocarbon deposits. The injectite structures can be difficult to image, however, with a better understanding of the subsurface and an increased amount of computational power, the injectite structures have become a target for seismic imaging and hydrocarbon exploration.

1.1 Problem description

This thesis aims at the imaging of subsurface injectite structures through the use of different acquisition geometries and migratory models. Both an elastic and an acoustic migration is to be evaluated.

1.1.1 Motivation and tasks

The identification of injectite structures is of a great interest in hydrocarbon exploration. Previously, there has been challenges in imaging these structures, due to their intrinsic geometry and geology. Considering the potential for hydrocarbon resources, an improved imaging of subsurface injectites carries huge potential for exploratory geophysics.

In this thesis, three different acquisition geometries will be compared in the imaging of subsurface injectite structures. The conventional streamer, the source over receiver geometry (SOR) and an ocean bottom survey (OBS). These geometries will be modeled by a finite difference method to create

shot gathers. The shot gathers will be used in a reverse time migration (RTM) to extrapolate an image of the subsurface. In the migration process, four different models will be considered. The reverse time migration will be performed by both an acoustic RTM class and an elastic RTM class. The difference in performance between the SOR geometry and the conventional streamer geometry in imaging the subsurface injectite structures is of special interest in this thesis.

1.2 Outline of thesis

A short overview of the chapters outlined in this thesis is provided.

1) **Introduction:** The subject of the thesis is introduced and a brief overview of the thesis is outlined.

2) **Theory:** Theory surrounding migration, the finite difference method and subsurface injectite structures is presented.

3) **Method:** The system for creating a subsurface image of injectite structures is presented.

4) **Results:** The most relevant results are presented.

5) **Discussion:** The results are analyzed and discussed.

6) **Conclusion:** Suggestions on further work is added and the thesis is concluded.

2 Theory

2.1 Seismic migration

The purpose of seismic migration is to move dipping reflections to their true position in the subsurface. The migration process also collapses the diffracted signals observed in the data. This process increases the spatial resolution, and in turn produces a seismic image of the subsurface. The migrated section is commonly displayed in time. One reason for this is that velocity estimation based on seismic or other data containing velocity information always has a limited accuracy. This error will propagate, and the depth conversion will contain the same inaccuracies. Interpreters of seismic data might also prefer to have the migrated section displayed in time, making a comparison to non-migrated data more convenient. However, using a spatial notation for the migrated section is also common, especially when one is analyzing synthetic data and an accurate velocity model is present.

In Figure 1, the effect of the migration process is sketched. Migration has multiple effects on a pre-migrated stack. Since the dip angle of the reflector is greater in the geological section than in the time section, migration steepens reflectors. Migration also reduces the length of the reflector, and moves the reflector in an updip direction.

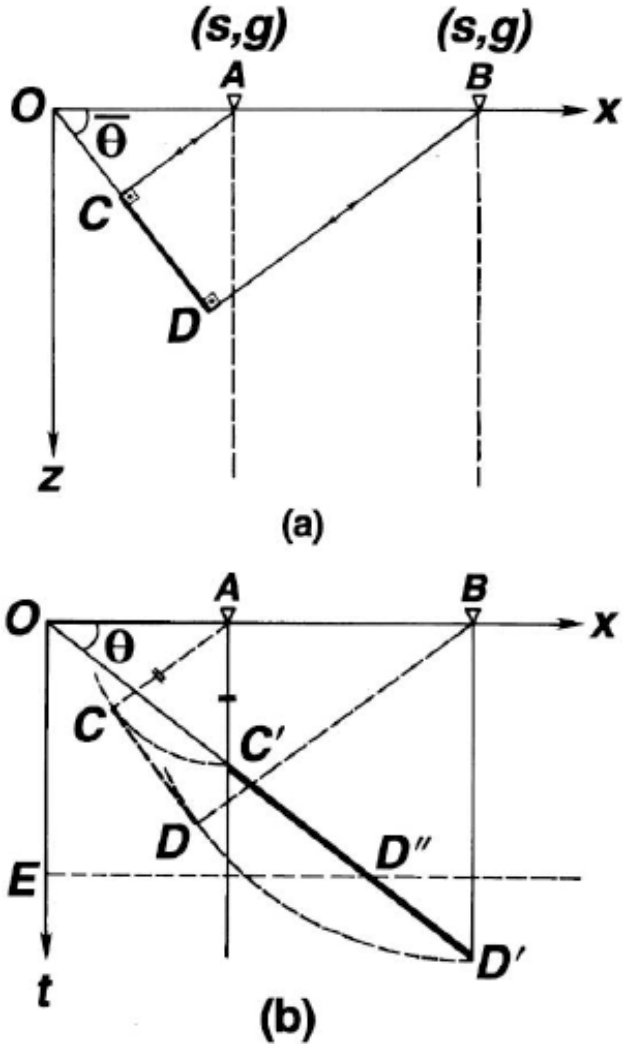

Figure 1: Here, the migration principle is illustrated. The relfection segment C'D' in ***(b)****, the pre-migrated stack, is steepened, shortened and moved into its true subsurface location. This migration is illustrated in* ***(a)****.[9]*

Chun and Jacewitz [1] derived formulas explaining the connection between the observed dip, $\frac{\Delta t}{\Delta x}$, in the non-migrated time section and the dip, $\frac{\Delta \tau}{\Delta x}$, measured on the migrated time section:

$$d_x = \frac{v^2 t}{4} \frac{\Delta t}{\Delta x} \tag{1a}$$

$$d_t = t\left(1 - \sqrt{1 - (\frac{v\Delta t}{2\Delta x})^2}\right) \tag{1b}$$

$$\frac{\Delta\tau}{\Delta x} = \frac{\Delta t}{\Delta x}\frac{1}{\sqrt{1 - (\frac{v\Delta t}{2\Delta x})^2}} \tag{1c}$$

Observe that the Equations 1 follow the migratory behaviour discussed in this section.

2.2 Reverse time migration (RTM)

The RTM is a type of depth migration using a temporal extrapolation rather than depth. The basic RTM takes two different forms. The first is used for stacked sections, where the imaging condition is is implicit at time zero. The other form is used for common source gathers, where the imaging condition is explicit. Using this form of RTM will give each point in the image space its own time stamp.

Since the stacked section implies the use of velocity information, P-wave and S-wave speeds cannot be imaged simultaneously when using a single stacked section. However, when using pre-stack data, one can obtain both P-wave and S-wave speeds when both vertical and radial components are recorded. The RTM was initially used for stacked sections. It later became much more common to use pre-stack data for both acoustic and elastic waves. Finite differences has dominated most implementations of the RTM, however, methods based on finite elements and ray tracing has also been explored.

The coupled second-order differential equations driving the RTM are to be solved simultaneously for both the forward and inverse problem. The theory is layed out by Sun and McMechan [10].

$$\rho\frac{\partial^2 u}{\partial t^2} = \frac{\partial}{\partial x}\left[\lambda(\frac{\partial u}{\partial x} + \frac{\partial w}{\partial z}) + 2\mu\frac{\partial u}{\partial x}\right] + \frac{\partial}{\partial z}\left[\mu(\frac{\partial w}{\partial x} + \frac{\partial u}{\partial z})\right] \tag{2a}$$

$$\rho\frac{\partial^2 w}{\partial t^2} = \frac{\partial}{\partial z}\left[\lambda(\frac{\partial u}{\partial x} + \frac{\partial w}{\partial z}) + 2\mu\frac{\partial w}{\partial z}\right] + \frac{\partial}{\partial x}\left[\mu(\frac{\partial w}{\partial x} + \frac{\partial u}{\partial z})\right] \tag{2b}$$

In equations 2 λ and μ are the Lamé parameters. The u and w notation describes the displacements in the x and z directions respectively. ρ is the density and t is time. In many cases, to reduce computational usage, the density is assumed to be constant. The Lamé parameters can then be described by the P- and S velocities.

$$\alpha = \left(\frac{\lambda + 2\mu}{\rho}\right)^{1/2} \tag{3a}$$

$$\beta = \left(\frac{\mu}{\rho}\right)^{1/2} \tag{3b}$$

The free-surface boundary conditions for the coupled differential equations are that normal stress is zero and that the tangential stress is zero.

$$(\alpha^2 - 2\beta^2)\frac{\partial u}{\partial x} + \alpha^2 \frac{\partial w}{\partial z} = 0 \tag{4a}$$

$$\frac{\partial u}{\partial z} + \frac{\partial w}{\partial x} = 0 \tag{4b}$$

The theory surrounding elastic reverse-time finite difference migration is layed out as by Sun and McMechan [10]. The forward problem is approached by first assigning a velocity distribution to each grid point. This is done for both compressional velocities and shear velocities. The source is thereafter put in two computational grids for two successive time steps. One for the vertical component, and one for the horizontal component, resulting in four initial grids. Both horizontal and vertical responses can now be found by applying the FD time marching scheme.

2.3 Finite differences synthetic modeling

In seismic analysis, numerical tools are crucial in order to generate a strong synthetic model. The finite difference method is often applied, due to its straight forward implementation when space and time have been discretized. The discretization of time and space allows for the discretization of the elastic wave equation. A time marching scheme can then be derived in order

to create a synthetic model that propagates in time. The finite difference equations can be seen in Appendix A.

The main drawback for the use of a FD modeling is its large use of computer memory. This especially can cause problems when one is carrying out a large scale seismic exploration. Modeling in 2D will in most cases be less computational expensive than modeling in 3D. However, as computational tools has become increasingly powerful, the memory challenges of the FD-modeling have become more manageable. This does not mean that this problem has gone away. When the seismic analyst is given more memory, increased spatial or temporal resolution is often desired. A method for decreasing memory requirements and computation times in the FD modeling is to use higher order approximations for the derivatives in the finite difference scheme.

The use of a staggered grid is also common to improve upon the efficiency of the FD-scheme. It works by storing the scalar variables (pressure, density etc.) in the center of the cell in the volume being modeled. Scalar variables as velocity is on the other hand stored at the faces of the cell. The use of the staggered grid is different from the collocated grid, where all variables are stored in the same grid cell location. There are particularly four qualities that is useful for seismic exploration that one finds with the use of staggered grids [6]. The staggered grid is stable for all values of Poisson's ratio, making it desired for marine exploration and other situations that deal with high Poisson's ratio materials. Secondly, grid anisotropy and grid dispersion are small and insensitive to Poisson's ratio. Thirdly, surface sources or buried sources can easily be defined and applied to the FD-scheme. Lastly, the free surface boundary conditions are also satisfied.

When carrying out a FD-modeling scheme, one has to use a finite elastic (or acoustic in the non-elastic case) model to define the model-space that is to be used in the FD simulation. The challenge one encounters with finite models are unwanted reflections from the model truncation boundaries. This issue is usually solved by adding a perfectly matched layer (PML). The PML is used as a layer placed around the outskirts of the computational grid. The PML is designed in a way that makes incident waves, coming from the non-PML region, not reflect back into the non-PML (region of computational interest) medium. The PML is often called a split PML. This is due to the wavefields being split into two unphysical fields in the defined PML region. This original definition has some disadvantages. Although implementation in many

cases is easy, the splitting PML requires more computing memory than other implementations. Improving upon this implementation, one can use a local PML. In a local PML, one uses regular wave equations in the modeling area and PML equations in the attenuating area, reducing the memory requirements. However, this implementation can be challenging due to the many different boundaries and corners. The non-splitting PML (NMPL) is often used to improve further upon the PML. This method has historically been considered too complex and not superior to the SMPL due to it requiring many computations. Recently the NMPL method has seen increased use. This is due to the NMPL being of a convolutional nature, taking advantage of not needing to split the field components in the attenuation region [3].

2.4 Sand injection complexes (high contrast anomalies)

When interpreting seismic images, the resolution used determines much of how well complex geometrical structures are imaged. Sand injection complexes are an example of this. Sandstone intrusions can be formed when faults and fractures are forced open by a naturally injected fluidized sand. When one has a sealed petroleum system, fractures and faults may promote a temporary or permanent fluid migration through a low-permability fine-grained strata, allowing for a upward migration of fluid. The sandstone intrusions can facilitate this migration if present, and since pro-fluid overpressure is not required to maintain dilatation, it may act as a reservoir for migrated hydrocarbons [8]. Grippa 2019 et. al. [7] analyzes these kinds of structures, and considers especially The Panoche Giant Injetion Complex (PGIC). This structure hosts one of the largest known sand injection complexes that is visible by simply observing the structure.

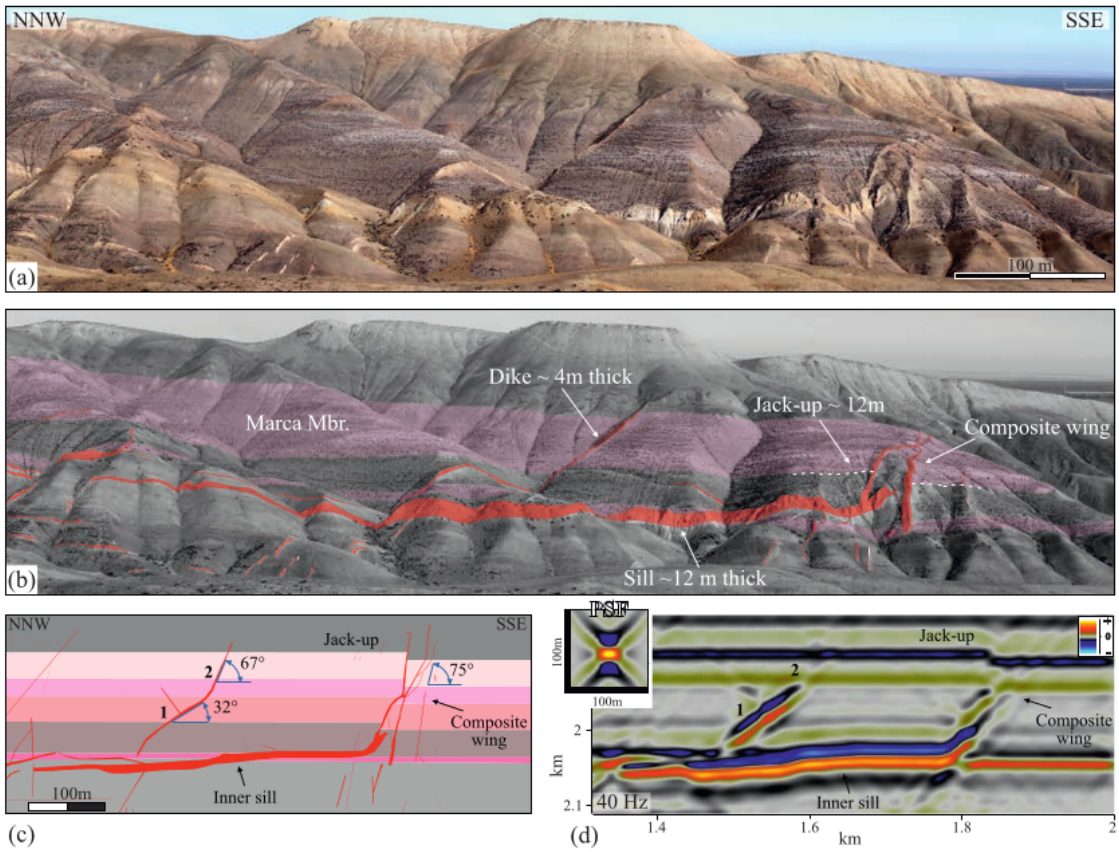

Figure 2: The Right Angle Canyon (RAC) of The Panoche Giant Injection Complex (PGIC). This is the more than 2 km long cliff section that Grippa et. al used for modeling resolvable intrusions for subsurface seismic analysis. a) an overview of the structure. b) Sandstone injectites are highlighted. c) Part of Grippas model of the RAC complex. d) Seismic image of the model in c).[7]

In Figure 2a) one can observe how these sandstone injectites may look. Further detail is applied in Figure 2b), where the true structure is highlighted. One of the challenges of imaging these complexes is the dip to the bedding. When the angle from the sandstone injectite to the bedding is low (approx. below 45°), the structure can be resolved. However, the sandstone injectites can in many cases have a high angle to the bedding. This makes imaging much more difficult, and increases the importance of sufficient azimuth coverage. The reality of this difficulty can be seen in Figure 2c). In Figure 2d)

one sees that after imaging the injectites, many highly dipping structures are hardly imaged.

Another challenge in the imaging of sandstone injectites is the resolution. The sandstone intrusions are not as uniform and structured as a regular subsurface layer with a low dipping angle. They can also be very slender in certain sections, increasing the importance of a finer grid. This can, especially for complex sandstone injectites, make 3D analysis computationally demanding.

3 Method

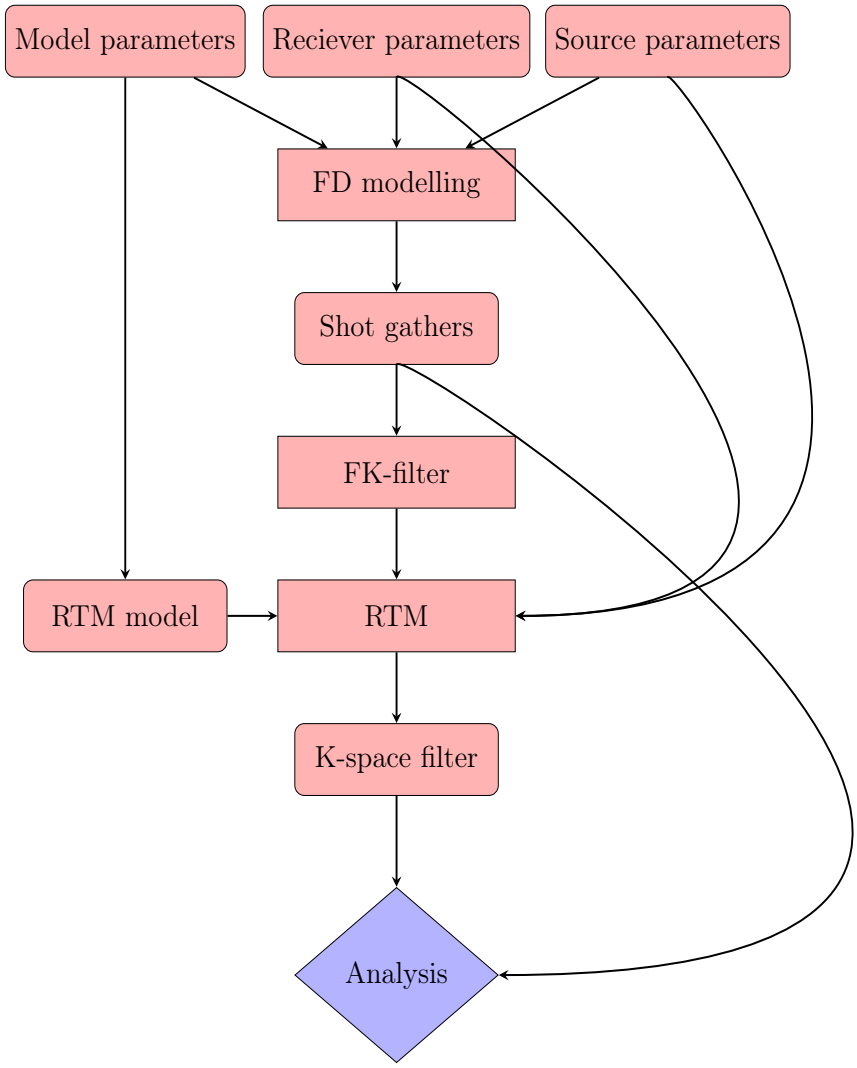

Figure 3: Flowchart illustrating a suggested process for generating a subsurface image of the injectite structures seen in Figure 4.

In this analysis, the desired result is creating a clear image of injectite structures by using a reverse time migration (RTM). Figure 3 depicts a suggested flow for creating a subsurface image of the injectite structures. In this sec-

tion, each part of the flowchart will be described in detail to paint a clear picture of how the subsurface image is generated.

3.1 Model

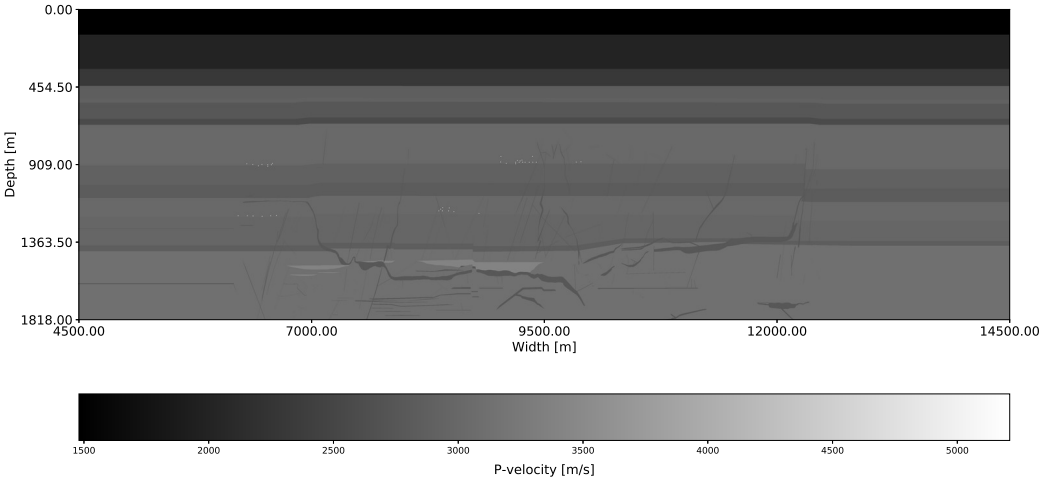

Figure 4: This figure is a picture of the model used to generate the shot-gathers through the use of the finite difference method.

In order for the finite difference process to create realistic and applicable shot gathers, an accurate model has to be defined. Grippa et al. designed a very accurate model of injectite structures that is to be used in this analysis [7]. The model was created from looking at The Right Angle Canyon (RAC) of The Panoche Giant Injection Complex. This injection complex can be seen in the earlier Figure 2. This is a detailed model created from an authentic case where injectite structures appear. Grippa then used the geometries found in the RAC to mirror these findings into a 2-D seismic model. This 2-D seismic model outlines P-velocity, S-velocity and density. The injectite geometries created by Grippa et al. is to be used in this analysis.

The model that is being used is detailed in Figure 4. The model is a classical layered maritime model, where the subsurface is divided into parallel structures of layered strata. The model depicted in Figure 4 is derived from P-velocity, however, models for both shear velocity and density were also defined. The injectite geometries, defined by Grippa et al. was merged with

this model of layered strata, resulting in a layered model with an injectite structure in the bottom-middle part of the model. Both models and RTM images analyzed in this thesis will therefore be magnified about the area of the model where the injectite structures reside. In this case, the x-axis was limited from $4500m$ to $14500m$.

3.2 Acquisition geometry

Three different acquisition geometries are to be considered in this analysis. The first method is the conventional streamer setup, followed by the source over receiver (SOR) method. The ocean bottom survey (OBS) is also to be considered.

3.2.1 Conventional streamer

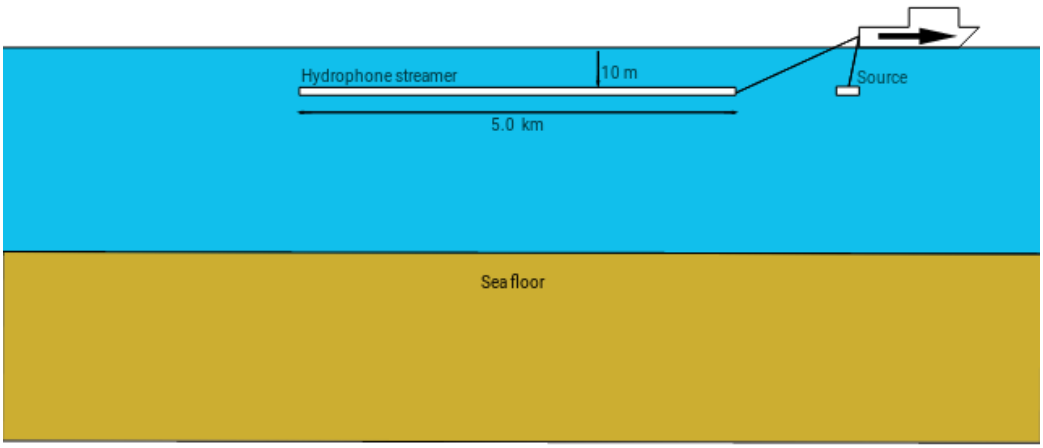

Figure 5: The conventional towed streamer geometry with a vessel piloting the hydrophone array and source.

The conventional towed streamer is the most common method used in exploratory geophysics. It is comprised of a hydrophone array placed horizontally under the sea surface. The hydrophone array is towed by a streamer vehicle that also deploys a source. Airguns are commonly used as an energy source, since the excreted energy is easily controlled and directed. The

streamer is then towed over the area of interest, while the source shoots energy into the subsurface. The reflections from the subsurface structures are then recorded by the hydrophone array. The data is then transferred to the streamer for further analysis. An illustration of the streamer acquisition geometry is depicted in Figure 5.

In this analysis the hydrophone streamer is $5km$ long, being submerged $10m$ under the ocean surface. The hydrophone array is composed of 501 receivers, spaced $10m$ apart. The source is also submerged $10m$, and it is positioned $50m$ horizontally from the hydrophone array.

One element that has to be noted is that the streamer is placed in the water layer. It follows that water cannot carry shear wave (S-waves), which means that some information from the subsurface reflections does not carry all the way to the receivers. This can somewhat be improved by using elastic modeling, allowing for S-to-P converted waves to be registered by the receivers.

3.2.2 Source over receiver (SOR)

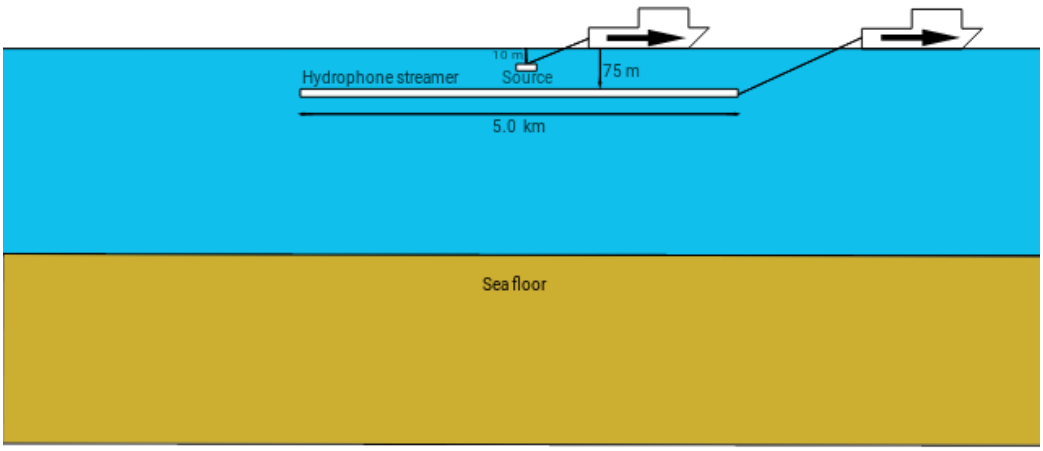

Figure 6: A source over receiver acquisition geometry, with one vessel towing the source, while another vessel tows the hydrophone array.

The source over receiver (SOR) geometry has recently been proposed as an improvement over the conventional streamer. Its advantage being an increase in near offset information. To explore this possibility, the image created with the SOR geometry is to be compared to the imaged created by the conventional streamer geometry. The SOR geometry takes use of two vessels: One vessel tows the hydrophone array, while the other vessel tows the source over the hydrophone array midpoint.

In this analysis, the source is $10m$ below the ocean surface, while the receiver array is $75m$ below the surface. The receiver array is composed of 501 receivers, spaced $10m$ apart. An illustration of the SOR geometry used can be seen in Figure 6.

3.2.3 Ocean bottom survey (OBS)

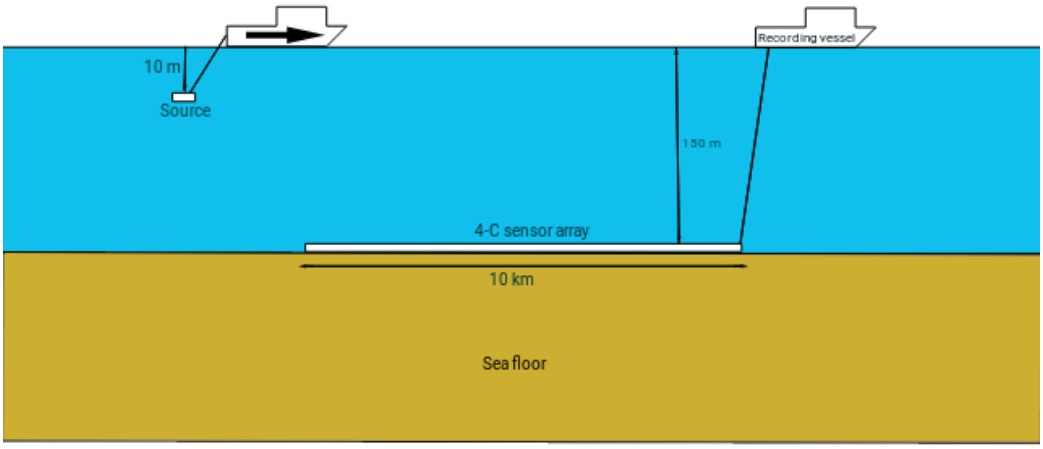

Figure 7: The ocean bottom survey geometry. One vessel is piloting the source, while an ocean bottom 4-C array sends the recorded data to a recorder vessel or buoy.

The last geometry that is to be considered in this analysis is the ocean bottom survey. It is commonly used when high detail and increased SNR is needed. OBS used ocean bottom nodes, usually connected by cable. These nodes then either connects to a buoy, or broadcasts to the buoy. The buoy

can then transmit the data by conventional means to the user for further analysis.

The OBS receivers used in this study is a four component (4C) receiver recording; x,y and z displacement, as well as pressure. These receivers are placed $150m$ below the ocean surface at the ocean floor. The OBS array is $10km$ long with a receiver every ten meters, making it a total of 1001 4C-receivers.

The choice of doubling the amount of receivers from the two other geometries was made to cater to the fact that the streamer and SOR hydrophone arrays would be towed a distance for each shot. To get a similar amount of azimuth in the OBS case, the amount of receivers were doubled. If one looks to Figure 4, the OBS nodes would be placed from $x = 5000m$ to $x = 15000m$ getting a sufficient azimuth coverage of the subsurface injectite complexes. An illustration of the OBS geometry can be seen in Figure 7.

One would expect that imaging by using an OBS should create a more detailed image, since all shear wave information is available. The information gathered by the use of this method cannot be compared equally to the two streamer methods, since the OBS geometry usually grants a more detailed result at a much higher expense.

3.3 Finite differences (FD) modeling

When one is conducting an analysis in seismic modeling, one has to have data to work with. In this analysis, synthetic seismic data is to be used. This data is to be created by the use of the finite difference method. In this application of the finite difference method, the source, receivers and model is defined. From this information, one extrapolate the shot gathers. The library used for all of the modeling and analysis in this thesis is the CSIM library developed in a collaboration between NTNU and AkerBP. This is a C++ library created for the purpose of sesmic imaging and modeling. As for computation, the high performance cluster MAUR was used.

The target of the finite difference modeling is in this analysis to create a certain amount of shot gathers. The program first defines a model. The model used is the same model as the one illustrated in Figure 4. The receiver geometry and the source position is also defined. One then sets the amount of

shots desired, as well as the number of grid cells between each shot. Through testing, it was found that approximately 190 shots were satisfactory to get sufficient seismic illumination of the subsurface structures. One shot was sent every $100m$ meters in the model. The number of time steps, time sampling and source parameters were also set. In addition, an NMPL was defined at the model boundaries.

For the conventional streamer and the SOR methods, local models were used. This is done to reduce the run-time and the computational requirements. Here, the model is split along the width-direction into several smaller models (only in the width-direction, the depth-dimension remains the same). At the end of the modeling, these local model results are stacked into a collective result. In the case of the OBS geometry, local models cannot be used. The OBS nodes are fixed at the ocean floor. This is opposed to the towed streamer methods, that can move throughout the water layer.

Having a high sampling frequency is required for numerical stability. It is therefore desired to downsample the data after the shot gathers have been calculated. This is mainly done to save memory and decrease run-time.

3.4 Pre-RTM filtering

It was found that using a F-K filter on the shot-gathers improves the detail of the structures of interest in the RTM images. F-K filtering was therefore applied to the shot gathers prior to running a reverse time migration. A frequency bandpass filter was applied with a passband $\vec{F}$. In the spatial k-domain, a bandpass filter was also applied with a passband $\vec{K}$.

$$\vec{F} = f_{nq}[0.05, 0.95] \tag{5}$$

$$\vec{K} = k_{nq}[0.05, 0.95] \tag{6}$$

In the equation above, f_{nq} denotes the Nyquist sampling frequency and k_{nq} denotes the Nyquist spatial sampling frequency.

3.5 Reverse time migration (RTM)

After the shot gathers have been modeled, these shots can be used in a reverse time migration process to generate an image of the subsurface. The image is in this analysis computed through the use of the CSIM libraries cross-correlation RTM process. This is to be done for both an acoustic and an elastic RTM.

Similarly to the FD data generation, the receiver, source and model parameters are defined. Direct arrivals at the shot gathers will then dominate in energy level. A mute is therefore applied to the direct arrivals of the shot gathers. A backwards source and a forward source is then defined in the RTM process, as well as an image object for the cross-correlation process. With this information established, a migration can be run and an image of the subsurface can be generated.

The model used for carrying out the RTM is crucial in generating a detailed image. Since an RTM tires to place the dips at their true subsurface locations, information detailing the subsurface geometry improve upon the detail of the image. One aspect that will be investigated in this thesis is the impact of detail in model. Four different models will be analyzed; an uniform model, a gradient model, a layered model and the true model seen in Figure 4.

The first model considered is the uniform model. This is a model where the geophysical parameters are set to the same value in all grid positions. In this analysis the density was set to $1000kg/m^3$, the P-velocity was set to $1480m/s$ and the S-velocity was set to $0m/s$. The uniform model was used to get a clear contrast between the different models used. This was done to highlight the importance of an accurate model when utilizing an RTM.

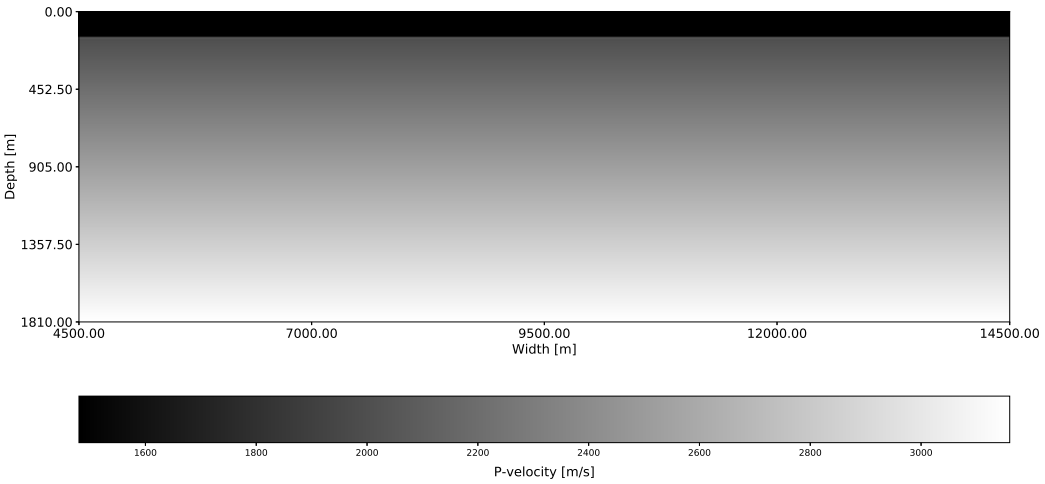

Figure 8: This figure illustrates the gradient model used in this analysis. It was created from the P-velocities of the gradient model.

The second model considered was a gradient model. An illustration of this model can be seen in Figure 8. The total width of this model is $19km$, however, the grid spacing in the generation of synthetic data was set to be ten. This means that there is one sample every 10 meters in the model. The RTM requires a cross-correlation of two fields. This can be computationally expensive for detailed grids. The models inserted into the RTM process is therefore resampled. It was assumed that one would have sufficient apriori information to know the depth of the water column and the geophysical characteristics of the top layer and the bottom layer. This model was to be used in an RTM for both the elastic and the acoustic case.

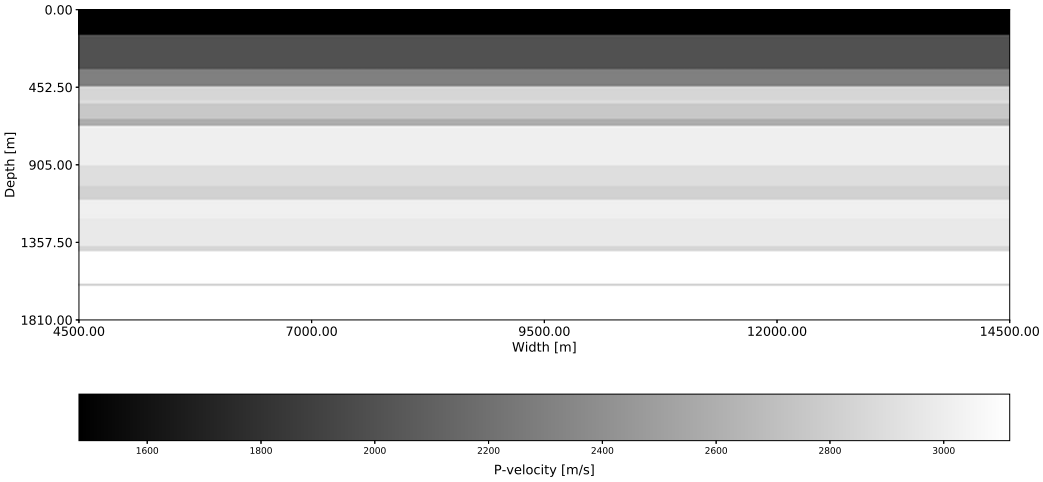

Figure 9: This figure illustrates the layered model used in this analysis. It was created from the P-velocities in the layered model.

The third model examined in this analysis, is the layered model. This model was designed to be very similar to the original model seen in Figure 4. However, it does not have the injectite structures embedded. This can be seen in Figure 9.

The last model that is to be compared is the true model, used in the initial FD modeling. The model is seen in Figure 4.

Acquisition geometry is also an important aspect of this analysis. All of the acquisition geometries discussed in Section 3.2 will be considered for both an acoustic and elastic RTM.

3.6 k-space filtering of RTM image

After an RTM image has been generated, there is still some k-domain noise that should be removed if one wants a clear subsurface image of the injectite structures. A MATLAB library called "MATGPR" was used for applying k-filters to the image. A 2-D filtering was applied through the use of one k-filter in the width-dimension and one k-filter in the depth-dimension. A bandpass k-filter was applied in the width dimension with a passband $\vec{K_x}$.

Another k-domain bandpass filter was applied in the depth dimension with a passband $\vec{K_y}$.

$$\vec{K_x} = k_{nq}[0.01, 0.90] \tag{7}$$

$$\vec{K_y} = k_{nq}[0.1, 0.90] \tag{8}$$

In the equation above k_{nq} denotes the Nyquist spatial sampling frequency.

4 Results

4.1 Finite Difference shot gathers

The shot gathers created through the use of the FD method is to be investigated to lay a foundation for the synthetic data used in this analysis.

4.1.1 Streamer shot gather

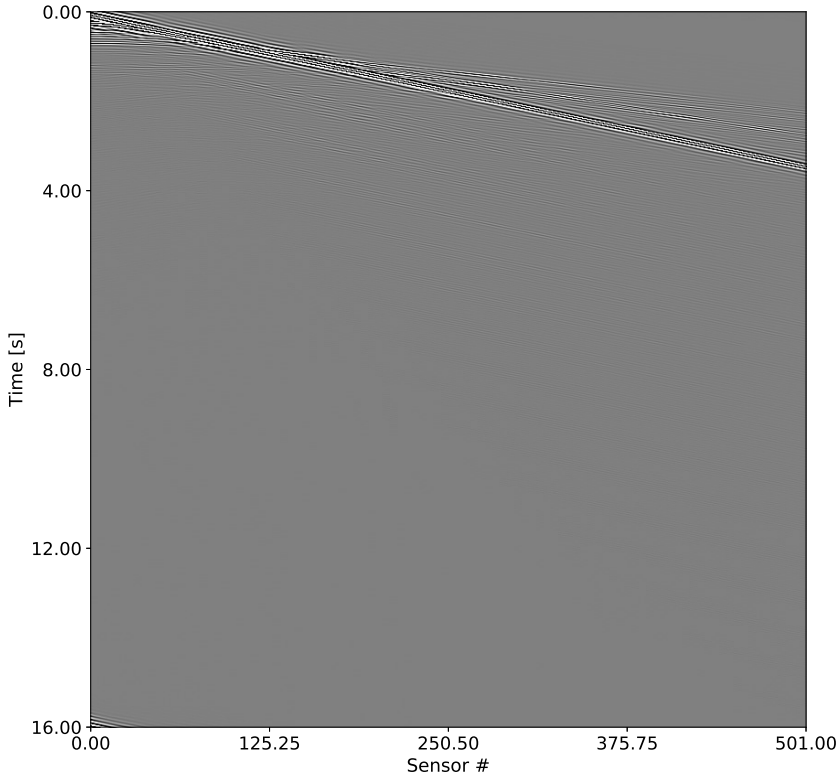

Figure 10: A shot gather captured at 501 hydrophones spaced 10 meters apart. The shot displayed in this figure originates from the 100th shot in the FD modeling.

The FD modeling was first preformed with a conventional streamer geometry. A resulting shot gather can be seen in Figure 10. This process was also done for a grid size that was 1:1 in comparison to the full model. The resulting

shot gathers were similar, however, a grid step of 10 meters was used for the majority of the analysis due to ease of computation. In creating the shot gathers, 16 seconds of time was modeled. This was the case for all acquisition geometries. This may have been a too large of a modeling window in order to optimize computational resources, but it was still used to ensure sufficient coverage.

4.1.2 SOR shot gather

The second iteration of FD modeling was aimed at the SOR (Source over receiver) geometry. 190 shot gathers was modeled and the 100th shot gather can be seen in Figure 11. One can observe that this geometry gives more data around low offset. This is due to the fact that the source is placed over the center of the hydrophone array. The direct arrivals will also dominate a possible RTM image in this case, so muting has to be applied to the two-sided structure of the direct arrivals in the shot gathers.

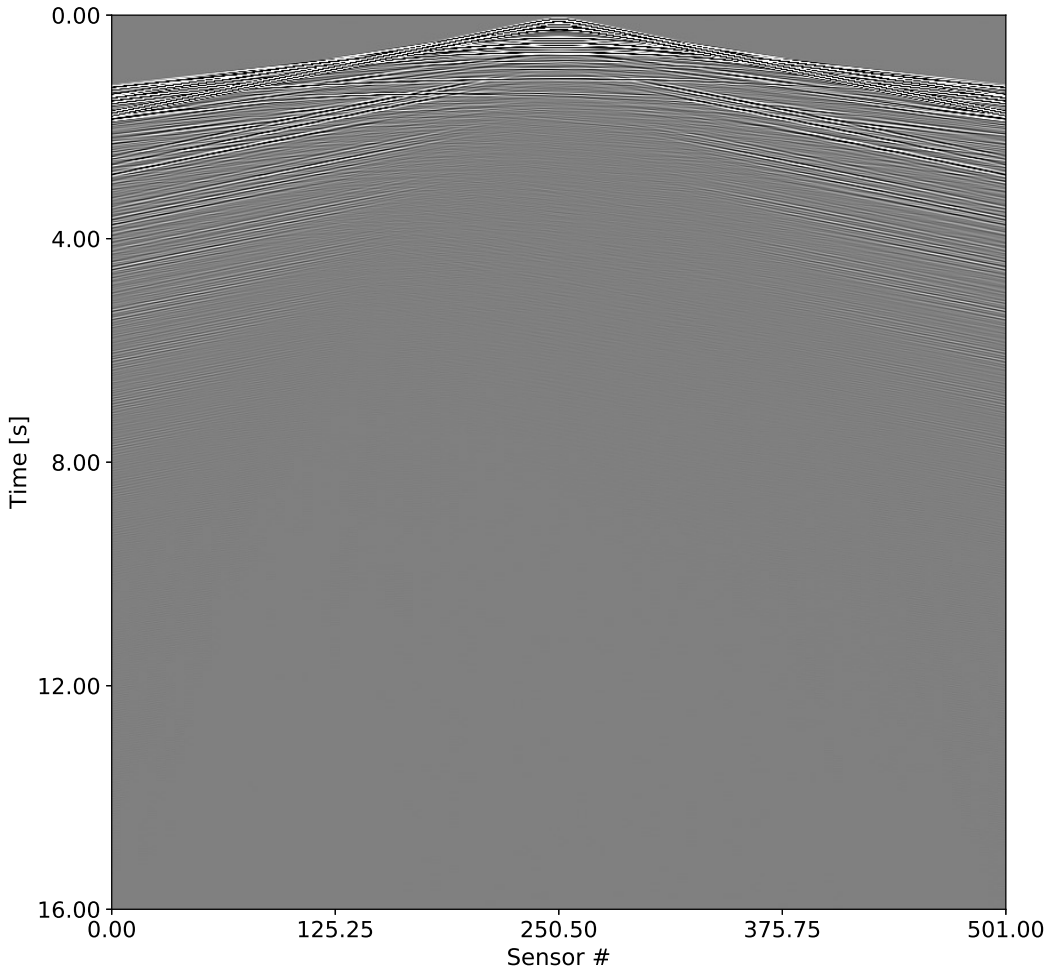

Figure 11: A shot gather captured at 501 hydrophones spaced 10 meters apart in a SOR geometry. The shot displayed in this figure originates from the 100th shot in the SOR FD modeling.

4.1.3 OBS shot gather

The last geometry that is to be modeled at the same $10m$ spaced grid with the OBS geometry. One of the synthetic shot gathers created can be seen in Figure 12. From looking at Figure 12 it is clear that the OBS shot gather data contains much more high energy information on the subsurface. Since an OBS geometry allows for direct S-wave information, one would expect the

OBS image detail to surpass the image detail of the two previously mentioned acquisition geometries, especially in the elastic case.

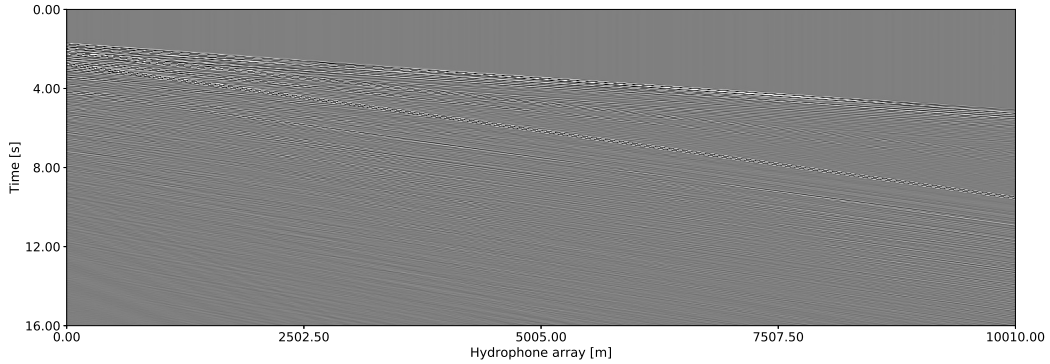

Figure 12: A shot gather captured at 1001 hydrophones spaced 10 meters apart in a OBS geometry. The shot displayed in this figure emerges from the 100th shot in the OBS FD modeling.

4.2 Uniform model

The first model that is to be investigated is the uniform model. This result is a point of comparison for the more detailed models. Both the acoustic and elastic case will be considered.

4.2.1 Acoustic migration

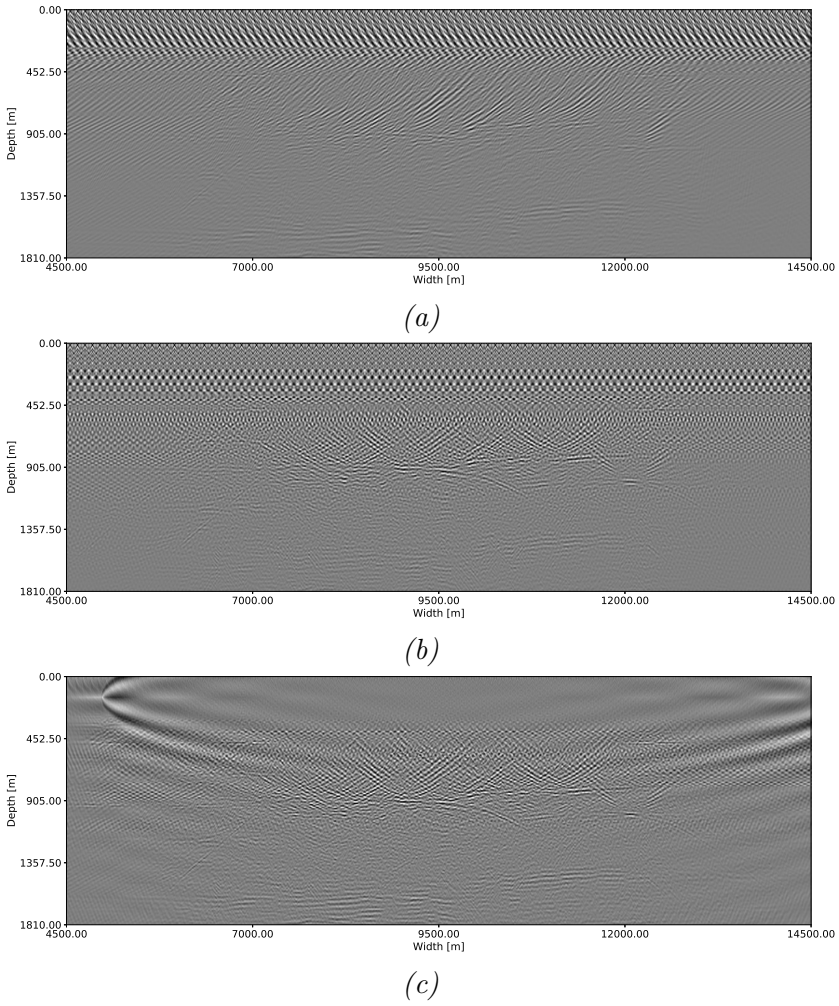

Figure 13: In all three figures the RTM was run with a uniform acoustic model. a) The resulting subsurface RTM image of the conventional streamer. b) The resulting subsurface RTM image for the SOR acquisition geometry. c) The resulting subsurface RTM image for the OBS acquisition geometry.

The shot gathers collected in the FD modeling was run in an RTM with a uniform acoustic model. The resulting RTM images can be seen in Figure 13. One can see from the figures that the injectite complexes of the original model

in Figure 4 is not clearly imaged by the acoustic RTM using a uniform model. This is to be expected to a certain degree, considering that the model used in the RTM gives little useful information for the migration process.

One can observe that there are some structures imaged in the middle of Figures 13 a), b) and c), however, this is not the true position of the injectites as seen in Figure 4.

4.2.2 Elastic migration

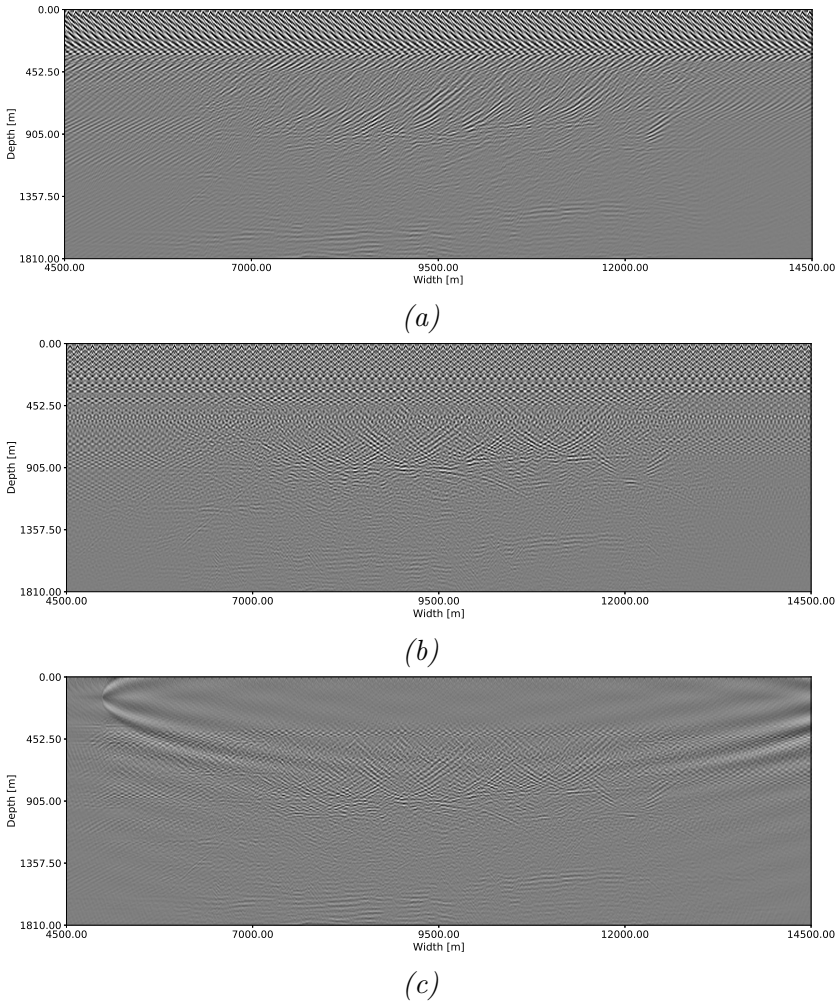

Figure 14: In all three figures the RTM was run with a uniform elastic model. a) The resulting subsurface RTM image of the conventional streamer. b) The resulting subsurface RTM image for the SOR acquisition geometry. c) The resulting subsurface RTM image for the OBS acquisition geometry.

In this section, the process from the previous section was preformed, however, in this case, a uniform elastic model was used. The resulting images are illustrated in Figure 14. One can see that there are no clear improvements

over the acoustic uniform model. This is to be expected, considering that the S-velocity in the uniform model was set to be zero. This leads to there not being any noticeable improvements in image detail over the acoustic case.

4.3 Gradient model

The next model that is to be evaluated is the gradient model. The gradient model used in the migration process is illustrated in the earlier Figure 8.

4.3.1 Acoustic migration

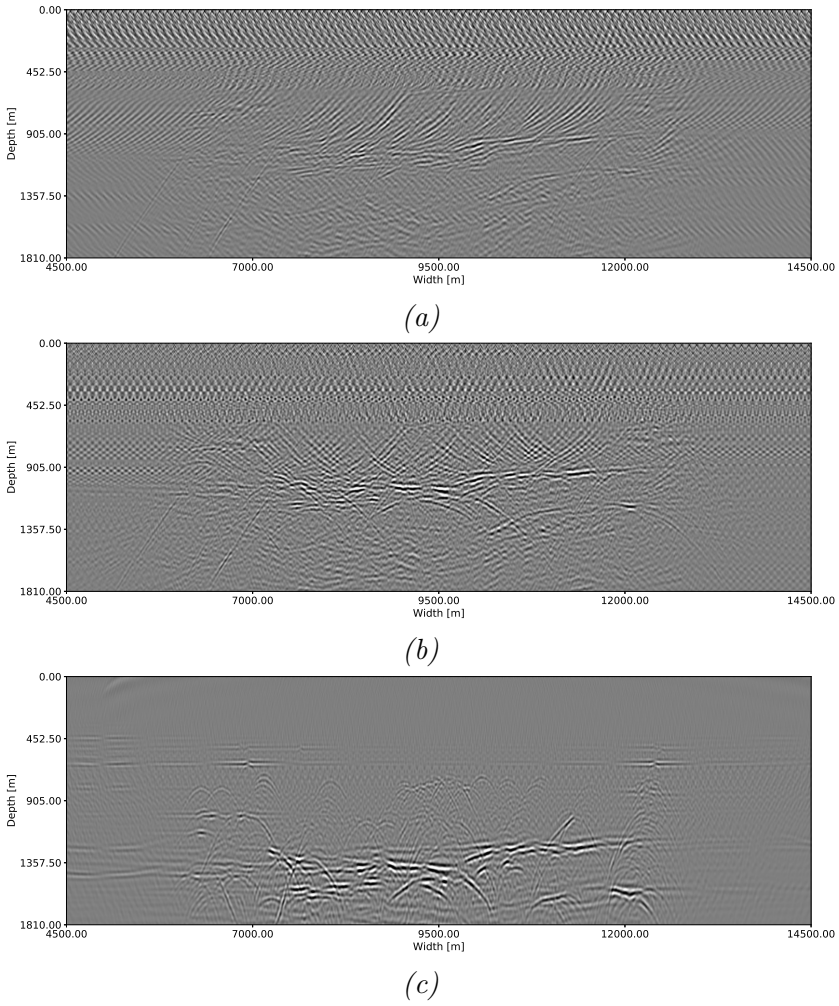

Figure 15: In all three figures the RTM was run with the gradient acoustic model. a) The resulting subsurface RTM image of the conventional streamer. b) The resulting subsurface RTM image for the SOR acquisition geometry. c) The resulting subsurface RTM image for the OBS acquisition geometry.

The resulting RTM images from using a gradient acoustic model in the migration process can be seen in Figures 15. Notice that the structures in the middle of the figures are more clearly imaged than the same structures seen

in Figures 13. Especially the OBS image in Figure 15c seems to contain a surprising amount of information despite it being generated from an acoustic RTM with a semi-accurate model in that of the gradient model.

However, the acoustic migration process still struggles to image the injectites accurately. One would expect that the injectite structures were returned to their true subsurface position as seen in Figure 4. The OBS case seems to be able to do this to a certain extent, however, the conventional streamer and the SOR geometry does not grant similar results to that of the OBS.

4.3.2 Elastic migration

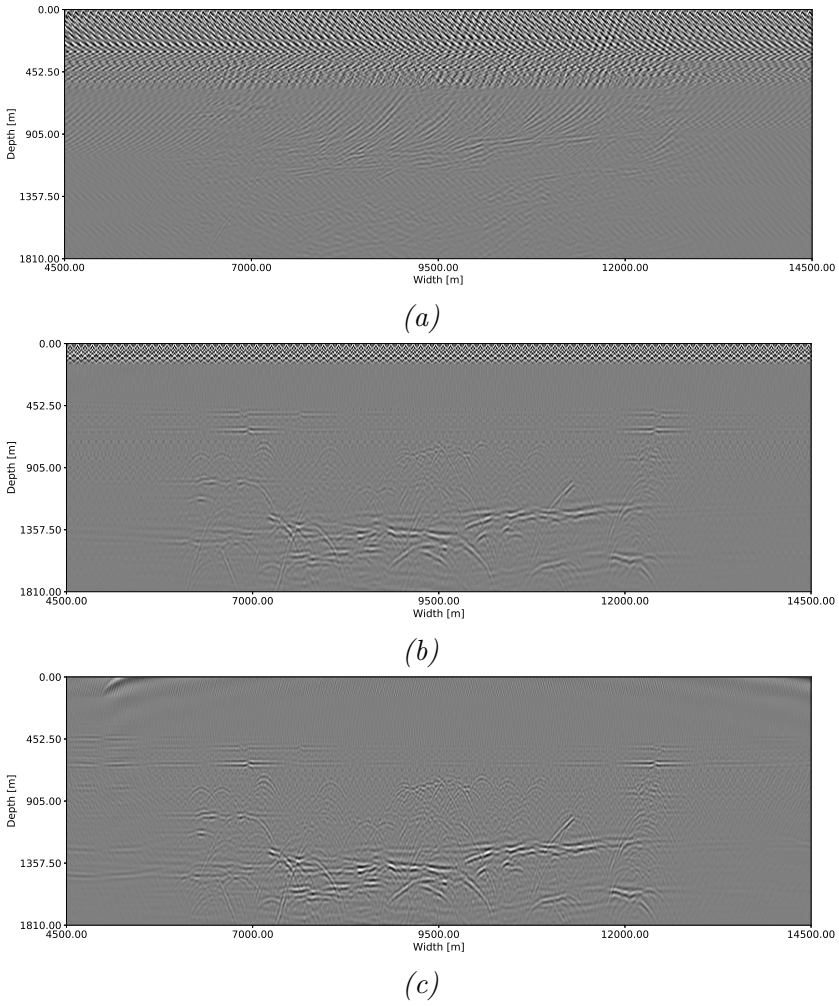

Figure 16: In all three figures the RTM was run with the gradient elastic model. a) The resulting subsurface RTM image of the conventional streamer. b) The resulting subsurface RTM image for the SOR acquisition geometry. c) The resulting subsurface RTM image for the OBS acquisition geometry.

The resulting images from a gradient elastic model can be seen in Figure 16. In these results one can definitely start to see a more accurate imaging of the subsurface injectite structures. First, one must look at 16a. Here, the

injectite structures are not easily identified. However, when we look to the result for the SOR geometry, seen in Figure 16b, the injectites are starting to be imaged at their true subsurface position. This may point towards certain advantages in using the SOR geometry over the conventional streamer when imaging subsurface injectite structures. The OBS result seen in Figure 16c is similar to that of the SOR result.

Seeing as the acoustic gradient model and the elastic gradient model granted different results after an RTM, one could expect that imaging of injectite structures is sensitive to elastic information.

4.4 Layered model

The third model examined in this analysis is the layered model. The model can be seen in Figure 9. Both the acoustic and elastic case will be considered.

4.4.1 Acoustic migration

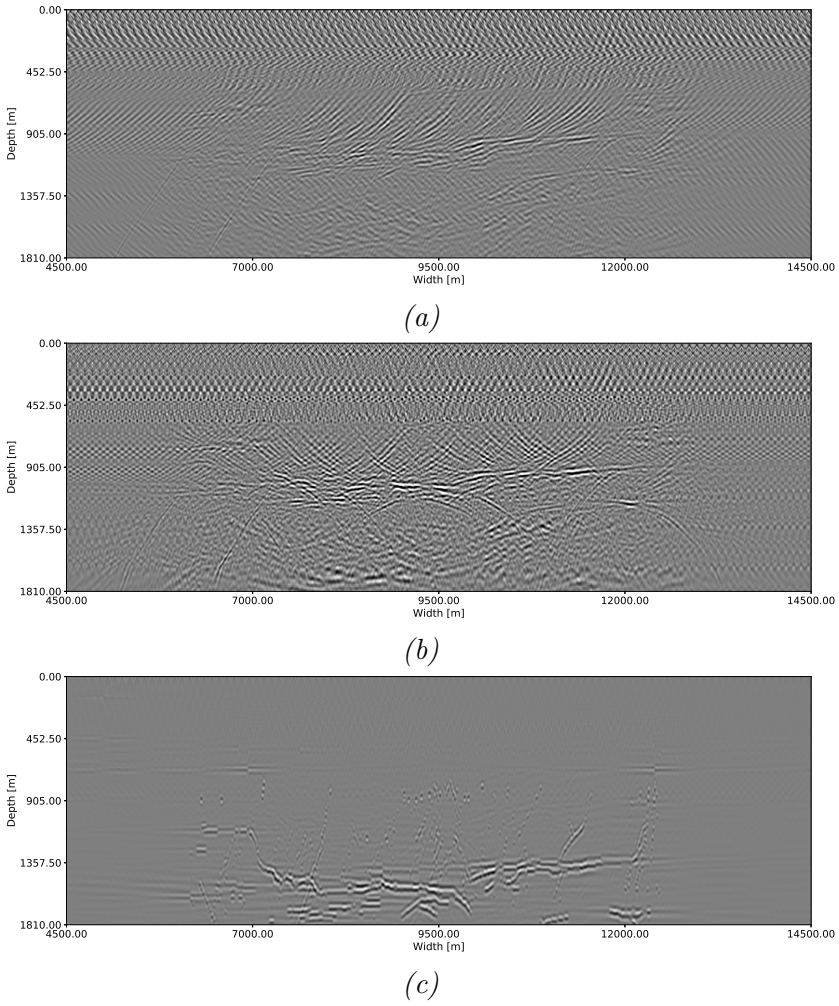

Figure 17: In all three figures the RTM was run with the layered acoustic model. a) The resulting subsurface RTM image of the conventional streamer. b) The resulting subsurface RTM image for the SOR acquisition geometry. c) The resulting subsurface RTM image for the OBS acquisition geometry.

The resulting RTM images of the subsurface for the acoustic layered model can be seen in Figure 17. Both the SOR and the conventional streamer results seem to follow that of the previous acoustic model analyzed. The

layered model used in this RTM is very close to that of the true model in Figure 4. It is therefore telling when the acoustic RTM still fails to return the dipping events to their true subsurface position. It seems that this result furthers the assumption of elastic information being of a vital importance when imaging injectite structures.

The acoustic RTM for the OBS geometry gives different results. This is seen in Figure 17c. This result seems very similar to that of the true model.

4.4.2 Elastic migration

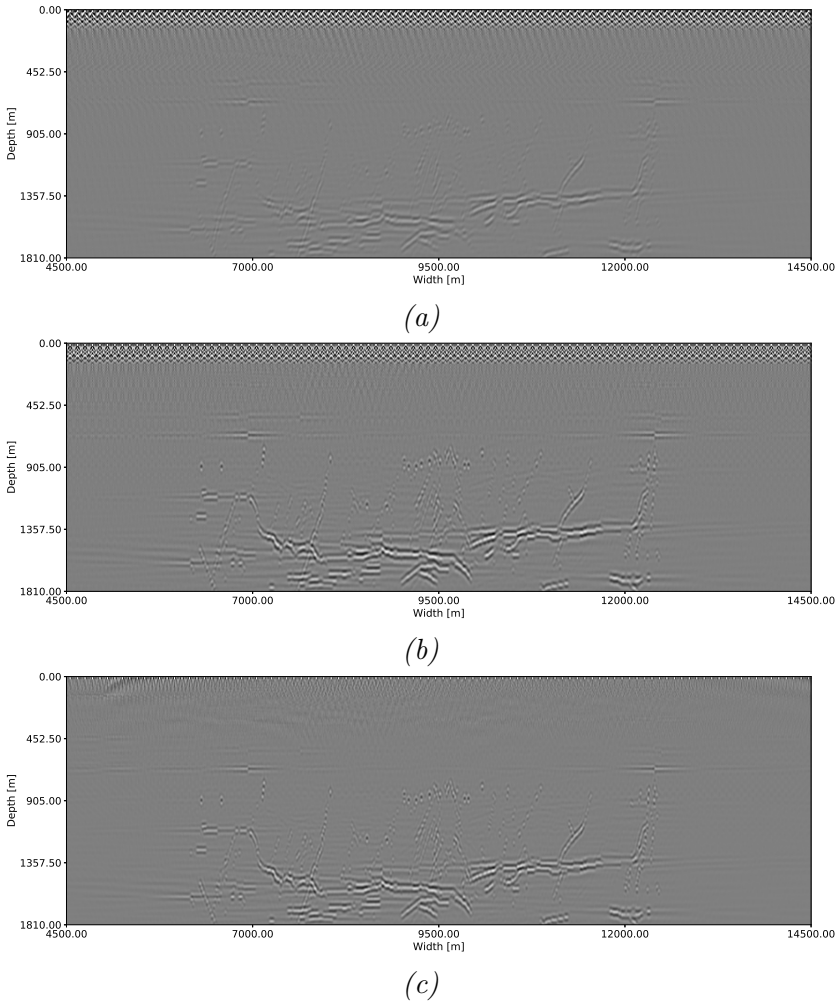

Figure 18: In all three figures the RTM was run with a layered elastic model. a) The resulting subsurface RTM image of the conventional streamer. b) The resulting subsurface RTM image for the SOR acquisition geometry. c) The resulting subsurface RTM image for the OBS acquisition geometry.

The layered model was then to be used in the case of an elastic RTM. The resulting subsurface images can be seen in Figure 18. One of the first events to observe is that of the conventional streamer. In the elastic gradient case,

the conventional streamer geometry did not produce a distinct image of the injectite structures. However, when a layered elastic model is applied, the injectite structures emerge from the RTM imaging process.

In the case of the SOR geometry, one can observe that the resulting image in Figure 16b is improved upon and the injectite structures are more sharply defined. The OBS geometry also produces a distinct image, through the use of the layered model in an elastic RTM.

4.5 True model

The last model to be evaluated is the true model. This is the original model used in the FD shot gather generation and it represents the true image of the subsurface. The model used can be seen in Figure 4.

4.5.1 Acoustic migration

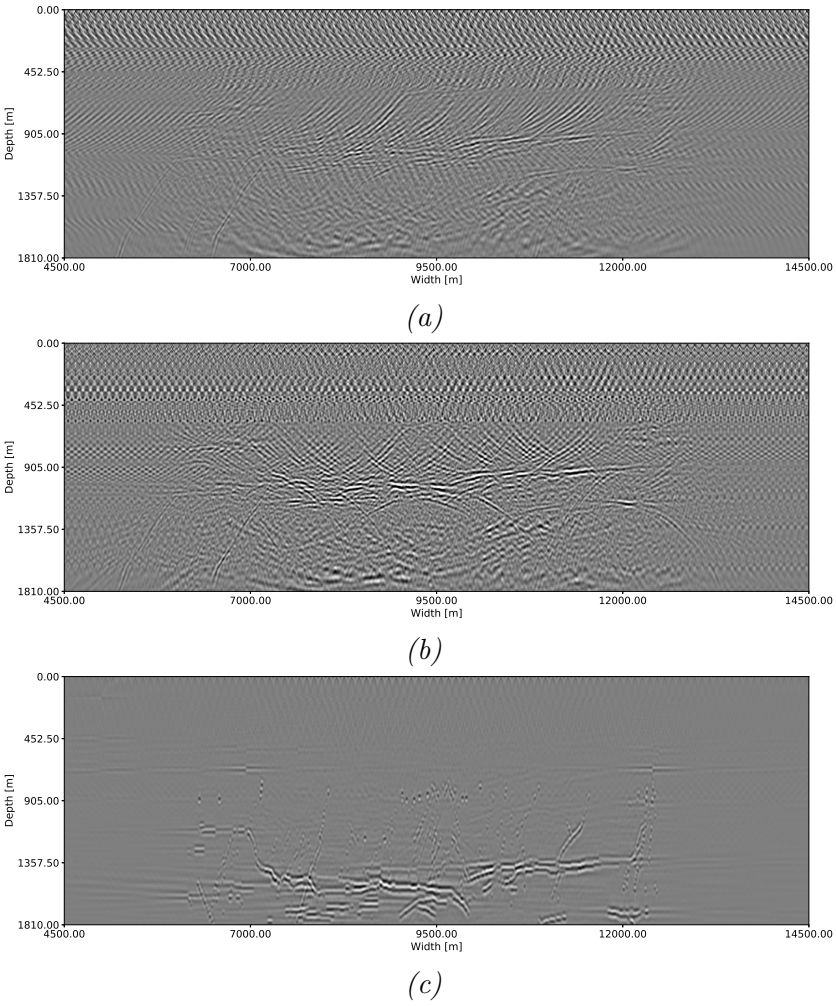

Figure 19: In all three figures the RTM was run with the a true acoustic model. a) The resulting subsurface RTM image of the conventional streamer. b) The resulting subsurface RTM image for the SOR acquisition geometry. c) The resulting subsurface RTM image for the OBS acquisition geometry.

The resulting subsurface images of a the true acoustic model can be seen in Figures 19. We can observe that the acoustic modeling continues to exhibit the same behaviour as in the previous acoustic RTM results. This happens

for the conventional streamer and the SOR geometry. The results emerging from the OBS geometry is very different. The OBS geometry seems to be able to image the injectite structures at their true subsurface positions.

4.5.2 Elastic migration

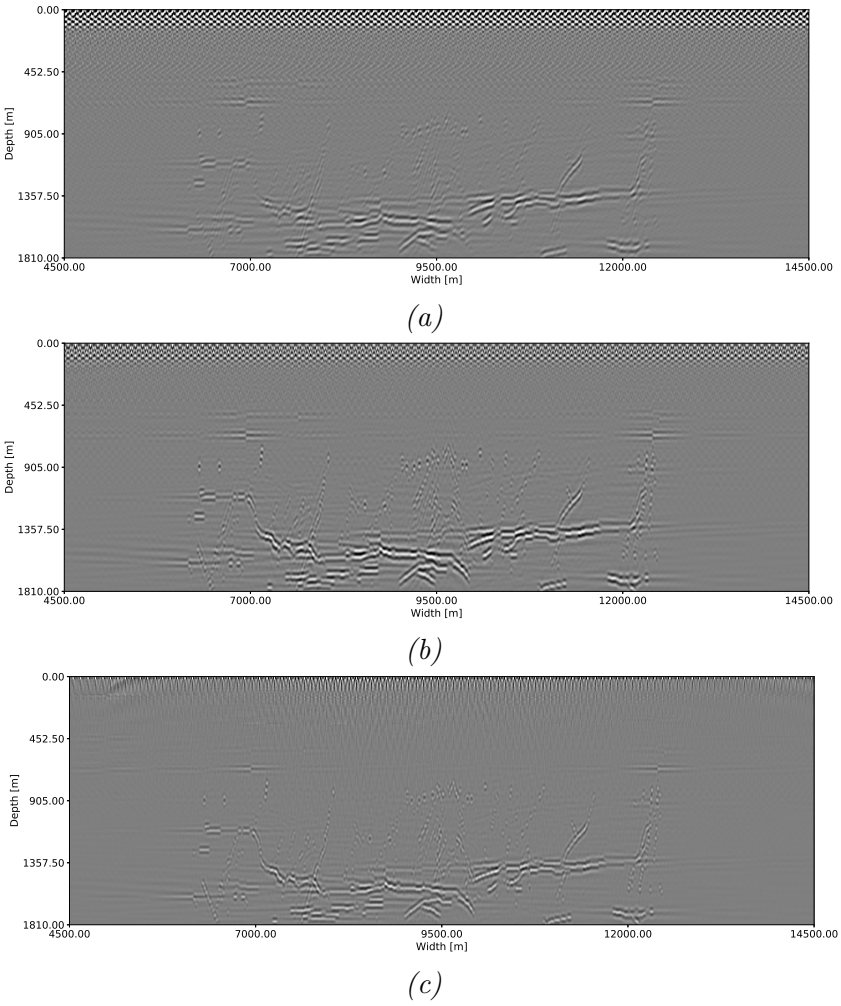

Figure 20: In all three figures the RTM was run with the true elastic model used in the initial FD modeling. a) The resulting subsurface RTM image of the conventional streamer. b) The resulting subsurface RTM image for the SOR acquisition geometry. c) The resulting subsurface RTM image for the OBS acquisition geometry.

The results from the running the elastic true model through the RTM can be seen in Figures 20. One would expect that with a true model, the subsurface

image of the injectite structures would improve. This is exactly what we see in Figures 20. The image from both conventional streamer and SOR improve with the use of a true model. The OBS image also seems to be more focused and sharp compared to the image extrapolated with the semi-accurate models.

5 Discussion

In this thesis, a procedure for imaging subsurface injectite structures was explored. An FD modeling was performed with the geological model seen in Figure 4. The shot gathers from the FD model was then used to image the subsurface through an RTM process. The findings has been presented in the result section and from these findings one gather some facts surrounding imaging of subsurface injectite structures. From the results gathered, there are multiple areas of interest that can be investigated. The importance of acquisition geometry and RTM model detail will be discussed. The effects of using an acoustic RTM versus an elastic RTM is also an important aspect of this analysis.

Acquisition geometry is an important part of this analysis. The results have been presented for the OBS geometry, the SOR geometry and the conventional streamer geometry. From the results it seems like the three different acquisition geometries preforms somewhat differently. The OBS geometry consistently outperforms the two other models. This happens for both the acoustic and elastic case, however, the OBS geometry drastically outperforms the two streamer methods in the case of an acoustic RTM. One would usually expect the OBS acquisition geometry to outperform the streamer geometries due to the availability of shear wave information. This is especially true for more complex geological structures such as high contrast injectite anomalies, where the shear wave information may contribute to fully unravel the reflections. However, this does not explain why the OBS geometry also supersedes the other geometries in the acoustic case. This may come from the fact that an almost doubled amount of receivers were used for the OBS case. This gives a greater coverage for subsurface reflections and it might catch reflections that a more narrow hydrophone array cannot.

Seeing as the OBS acquisition method is a much more expensive procedure, it is also interesting to see the compared performance of the SOR method and the conventional streamer. For these geometries, only the elastic RTM granted useful results. These results will therefore be compared when evaluating the difference in performance. If one looks to Figure 16, one can see the results from a gradient model being used in an elastic RTM. Here, the conventional streamer is not able to clearly migrate the dipping events in the injectite structures seen in Figure 4. However, the SOR geometry is to a

certain degree able to do this. The gradient model seen in Figure 8, is not a very accurate model compared to that of the layered model or the true model. Despite this it seems that it performs similarly to that of the OBS geometry in an elastic RTM using the gradient model. In the following section, an elastic RTM is run with the layered model. The results are seen in Figure 18. Now one can observe that the conventional streamer geometry is also able to create a faint image of the subsurface injectite structures. However, it is clear that the SOR geometry makes a more distinct and clear image. This trend continues when the true model is used in the elastic RTM. The difference in performance may come from the increase of near offset data in the SOR case. These findings suggest that there might be advantages to using the SOR geometry over the conventional streamer geometry when imaging subsurface injectite structures.

The importance of detail in the model used in the migration is also an important part of this thesis. Four different models were investigated in this analysis. The uniform model does not preform well in an RTM where the subsurface geology is non-uniform. However, it serves an important role in establishing the impact of model detail in imaging of subsurface injectite structures. The gradient model was an improvement on the uniform model. Despite it not being a very accurate model, it still improved upon the results from the uniform model. This is especially true for the elastic case. If one looks to Figure 16, both the OBS and the SOR geometry is able to somewhat image the injectite structures at their true subsurface position. This trend continues for the layered model, which is a subsurface RTM model that is much closer to the true model used in the FD modeling. The results seen in Figure 18 further improves upon the results from using the gradient model. In this case, the elastic RTM is able to image the injectite structures for all acquisition geometries. However, the conventional streamer geometry does not grant as clear an image as the other two methods. The last model used in the migration process is the true subsurface model seen in Figure 4. Similarly to the uniform model, the true model was used as a point of comparison for the importance of model detail. If a seismic analyst had the true subsurface model, imaging would not necessarily be needed in the first place. However, it is of interest to see the improvement of the subsurface image when a true model is applied to the migration. If one compares the results in Figures 18 and 20, an increase in detail is especially seen in the case of the conventional streamer geometry. The image quality of the subsurface injectite

structures also seem to improve with the OBS and SOR geometry. Though this improvement is not as considerable as with the conventional streamer geometry.

Model detail is of great importance when one desires to image subsurface structures. This analysis confirms that this also is the case for subsurface injectite structures. The detail of subsurface image seems to improve drastically when an layered model is introduced. The findings indicates that using a strong model in the migration is important to get an accurate depiction of the injectite structures.

Subsurface images have been produced by both an acoustic and an elastic RTM process. From looking at the results from the acoustic RTM in Figures 13, 15, 17 and 19, only the OBS geometry is able to reconstruct the injectite structures at their true subsurface positions. From looking at the elastic case in Figures 14, 16, 18 and 20, we see that the injectite structures are imaged at their true subsurface position for the more accurate models. A clear difference in results emerges from this analysis, especially when the SOR or conventional streamer geometry is applied. In the case of the two streamer methods, none of the acoustic RTMs produced a satisfactory subsurface image. This may point towards an importance of elastic information for both streamer geometries. Still, this does not explain why the OBS geometry perform much better for all the acoustic RTMs that have been computed. An explanation could be that the OBS sensor array is double the size of the sensor array used in the streamer geometries. The use of local models in the two streamer geometries might also have contributed to this development.

There are multiple limiting factors to this thesis. The entirety of the analysis has been conducted with synthetic data. In practice, forces such as geological inhomogeneity and environmental noise increases the complexity of the imaging process. Another important factor is the FD modeling. In this thesis, the shot gather data was generated on a downsampled model. Since the injectite structures can be very slender, some inaccuracies might emerge. These inaccuracies might have been avoided if the data was generated on a finer grid.

6 Concluding remarks

6.1 Further work

In order to truly understand the differences between the conventional streamer and the SOR streamer when it comes to imaging of subsurface injectite structures, further research is needed. Past studies have focused on the challenges of imaging due to steep sections in the injectite structures [7]. The use of an SOR geometry for data gathering is still an area that is unexplored when it comes to the imaging of injectite structures. Further work focusing on different SOR geometries is an area of interest that could impact the imaging of subsurface injectite structures.

Through this analysis, there are still questions surrounding the use of an acoustic RTM versus an elastic RTM. The acoustic migration is the method that is predominantly used in industry. This is due to the increased computational demand when one is running an elastic RTM. It is therefore desirable to improve upon the acoustic migration when imaging subsurface injectite structures. In future studies, there are multiple areas of interest. One could use a larger local model or adopt the full model when generating the shot gathers and migrating the data. Deploying a hydrophone array with more sensors is also a possible area of research. Future work could also benefit from using a finer grid in the FD modeling.

6.2 Conclusion

The thesis focused on the imaging of subsurface injectite structures. A geological model of layered strata containing injectite structures was defined. The imaging has been done through the use of three different acquisition geometries; the conventional streamer, the SOR geometry and an OBS geometry. Each acquisition geometry created a number of shot gathers that were migrated to create a subsurface image. The elastic migration granted satisfactory results for all acquisition geometries. However, the acoustic migration struggled to migrate the shot gathers for the conventional streamer and the SOR geometry.

The detail of the model used in the migration was an important part of

this thesis. Four different models were used in both an acoustic and an elastic migration for all three acquisition geometries. The results indicate that model detail is of great importance when imaging injectite structures. An increased model detail significantly increased the detail of the subsurface injectite image.

The SOR geometry was of special interest in this thesis. When an elastic migration was applied, the SOR geometry outperformed the conventional streamer geometry. The results suggested that using an SOR geometry over a conventional streamer geometry grants a more detailed subsurface image of injectite structures. In this analysis the SOR geometry performed close to that of the OBS when elastic migration was applied. In cases where an OBS is financially unfeasible, an SOR geometry may be advantageous in the imaging of subsurface injectite structures.

Appendix

A Finite difference equations

The finite difference equations are derived by Levander [6]. The first step is to discretize the x, z and t variables. Depending on the definition of the staggered grid

$$x = mh \tag{9a}$$

$$x = (m \pm \frac{1}{2})h \tag{9b}$$

$$z = nh \tag{10a}$$

$$z = (n \pm \frac{1}{2})h \tag{10b}$$

$$t = l\Delta t \tag{11a}$$

$$t = (l \pm \frac{1}{2})\Delta t \tag{11b}$$

where h is the grid spacing, and Δt is the time sample period. The difference equations can now be defined as

$$\begin{aligned} &D_t^+ u_t(m, n, l - 1/2) = \\ &1/\rho(m, n)[D_x^- \tau_{xx}(m + 1/2, n, l) + D_z^- \tau_{xz}(m, n + 1/2, l)] \end{aligned} \tag{12a}$$

$$\begin{aligned} &D_t^+ w_t(m + 1/2, n + 1/2, l - 1/2) = \\ &1/\rho(m + 1/2, n + 1/2)[D_x^+ \tau_{xz}(m, n + 1/2, l) + D_z^+ \tau_{zz}(m + 1/2, n, l)] \end{aligned} \tag{12b}$$

$$\begin{aligned} &D_t^+ \tau_{xx}(m + 1/2, n, l) = [\lambda(m + 1/2, n) + 2\mu(m + 1/2, n)] D_x^+ u_t(m, n, l + 1/2) \\ &+ \lambda(m + 1/2, n) D_z^- w_t(m + 1/2, n + 1/2, l + 1/2) \end{aligned} \tag{12c}$$

$$D_t + \tau_{xz}(m, n+1/2, l) = \mu(m, n+1/2)[D_z^+ u_t(m, n, l+1/2) + D_x^- w_t(m+1/2, n+1/2, l+1/2)] \tag{12d}$$

$$D_t^+ \tau_{zz}(m+1/2, n, l) = [\lambda(m+1/2, n) + 2\mu(m+1/2, n)] \cdot D_z^- w_t(m+1/2, n+1/2, l+1/2) + \lambda(m+1/2, n) D_x^+ u_t(m, n, l+1/2) \tag{12e}$$

In the equations above, D_t^+ is the forward difference operator in time. $D_x^\pm$ and $D_z^\pm$ are the forward and reverse difference operators in the spatial domain, where the sign describes the centering of the difference operator about the updated quantity. An example, as illustrated by Levander [6], is the spatial derivative of the normal stress component used for obtaining an updated particle velocity.

$$D_x^- \tau_{xx}(m+1/2, n, l) = -c_2 [\tau_{xx}(m+3/2, n, l) - \tau_{xx}(m-3/2, n, l)] + c_1 [\tau_{xx}(m+1/2, n, l) - \tau_{xx}(m-1/2, n, l)] \tag{13}$$

c_1 and c_2 are respectively the inner and outer coefficients for the fourth order approximation to the first derivative. They are valued at respectively $9/8$ and $1/24$.

References

[1] Chun and Jacewitz, 1981, Chun, J.H. and Jacewitz, C., 1981, Fundamentals of frequency-domain migration: Geophysics, 46, 717–732.

[2] Chang, W. and McMechan, G. (1987). Elastic reverse-time migration. GEOPHYSICS, 52(10), pp.1365-1375.

[3] Qin, Z., Lu, M., Zheng, X., Yao, Y., Zhang, C. and Song, J. (2009). The implementation of an improved NPML absorbing boundary condition in elastic wave modeling. Applied Geophysics, 6(2), pp.113-121.

[4] Virieux, J. (1986). P-SVwave propagation in heterogeneous media: Velocity-stress finite-difference method. GEOPHYSICS, 51(4), pp.889-901.

[5] Virieux, J. (1984). SH-wave propagation in heterogeneous media: Velocity-stress finite-difference method. GEOPHYSICS, 49(11), pp.1933-1942.

[6] Levander, A. (1988). Fourth-order finite-difference P-SV seismograms. GEOPHYSICS, 53(11), pp.1425-1436.

[7] Grippa, A., Hurst, A., Palladino, G., Iacopini, D., Lecomte, I. and Huuse, M. (2019). Seismic imaging of complex geometry: Forward modeling of sandstone intrusions. Earth and Planetary Science Letters, 513, pp.51-63.

[8] Hurst, A., Scott, A., Vigorito, M., 2011. Physical characteristics of sand injectites. Earth-Science Reviews, v. 106, pp. 215–246.

[9] Geary, A. (2014). Migration principles - SEG Wiki. [online] Wiki.seg.org. Available at: https://wiki.seg.org/wiki/Migration_principles#/media/File:Ch04_fig1-1.png [Accessed 5 Jul. 2019].

[10] Sun, R. and McMechan, G. (1986). Pre-stack reverse-time migration for elastic waves with application to synthetic offset vertical seismic profiles. Proceedings of the IEEE, 74(3), pp.457-465.

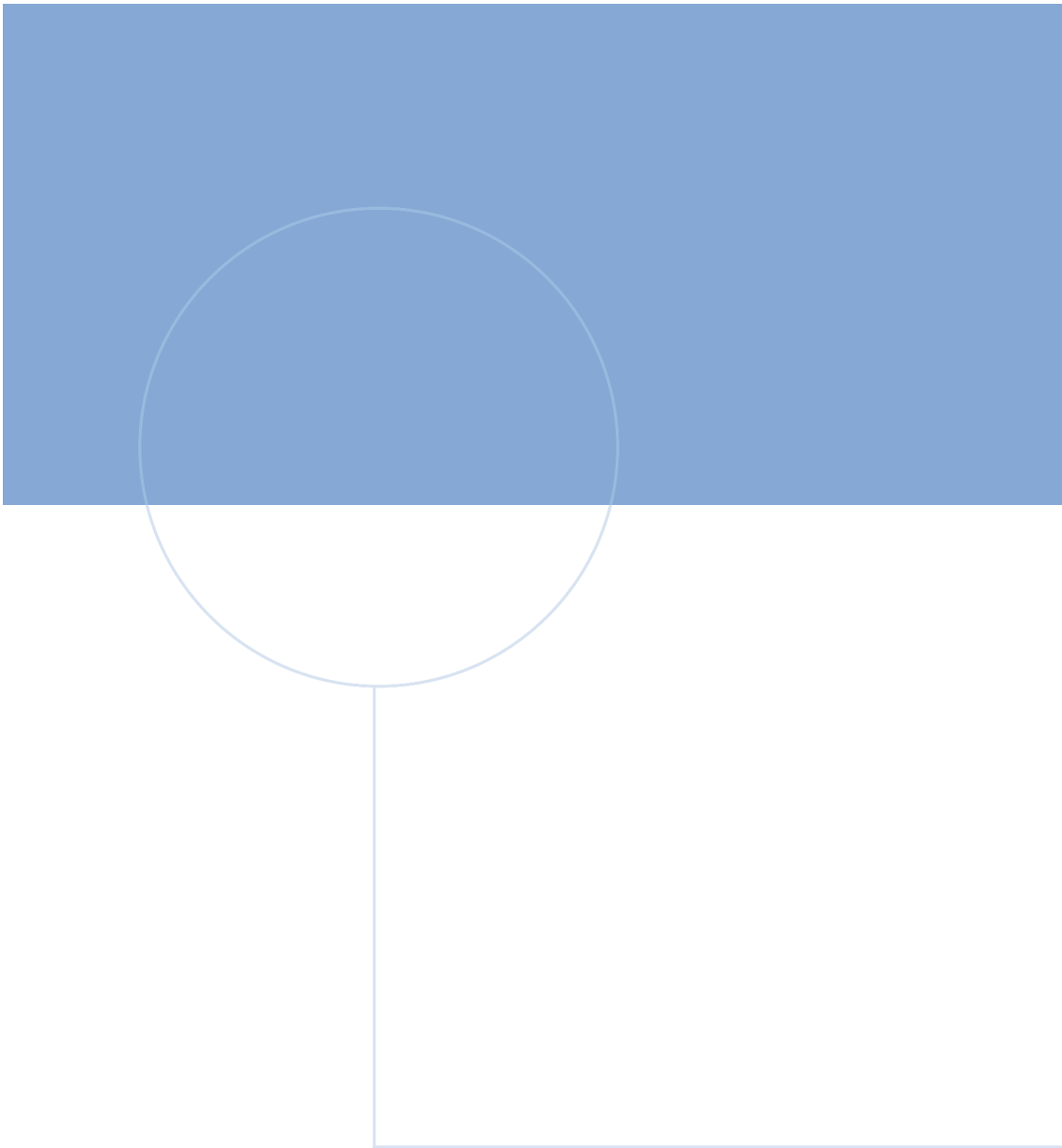

NTNU
Norwegian University of
Science and Technology